A hedonic orexigenic subnetwork within the human hippocampus

Daniel A. N. Barbosa
Perelman School of Medicine, University of Pennsylvania https://orcid.org/0000-0001-7272-1446
Sandra Gattas
Perelman School of Medicine, University of Pennsylvania
Juliana S. Salgado
Stanford University School of Medicine
Fiene Marie Kuijper
Perelman School of Medicine, University of Pennsylvania
Allan R. Wang
Perelman School of Medicine, University of Pennsylvania
Yuhao Huang
Stanford University School of Medicine
Bina Kakusa
Stanford University School of Medicine
Christoph Leuze
Stanford University School of Medicine https://orcid.org/0000-0003-4564-8014
Artur Luczak
Canadian Center for Behavioural Neuroscience https://orcid.org/0000-0002-4929-5781
Paul Rapp
Uniformed Services University
Robert C. Malenka
Stanford University https://orcid.org/0000-0002-5428-5211
Kai J. Miller
Mayo Clinic
Boris D. Heifets
https://orcid.org/0000-0003-1474-0379
Cara Bohon
Stanford University School of Medicine
Jennifer A. McNab
Stanford University School of Medicine https://orcid.org/0000-0002-1763-0792
Casey H. Halpern (Casey.Halpern@Pennmedicine.upenn.edu)
Stanford University

Biological Sciences - Article

Keywords: appetitive processing, feeding behavior, obesity, binge eating, food addiction, food anticipation, resting-state fMRI, tractography, brain-clearing, iDISCO, cortico-subcortical evoked potential, low-frequency, theta power, hippocampal area, melanin-concentrating hormone, lateral hypothalamic area

Posted Date: February 17th, 2022

DOI: https://doi.org/10.21203/rs.3.rs-1315996/v1

Version of Record: A version of this preprint was published at Nature on August 30th, 2023. See the published version at https://doi.org/10.1038/s41586-023-06459-w.

Abstract

Only recently has the rodent hippocampus been implicated in orexigenic appetitive processing[1,2]. This function has been found to be mediated at least in part by lateral hypothalamic inputs involving an orexigenic neuropeptide, melanin-concentrating hormone[3]. This circuit remains elusive in humans. Here, we combine tractography, intracranial electrophysiology, cortico-subcortical evoked potentials, and brain-clearing 3D histology to identify an orexigenic circuit involving the lateral hypothalamus converging in a hippocampal subregion. We found that low-frequency power is modulated by sweet-fat food cues and this modulation was specific to the dorsolateral hippocampus. Lastly, structural and functional analyses of this circuit in a human cohort exhibiting dysregulated eating behavior revealed connectivity that was inversely related to body mass index. Collectively, this multimodal approach describes an orexigenic subnetwork within the human hippocampus implicated in obesity and related eating disorders.

full text

Orexigenic appetition relies on the integration of sensory, interoceptive and hormonal signals to govern consummatory behaviors[1,4]. Dysregulation of this process leads to maladaptive eating behavior such as binge eating and even obesity[5]. Studies in rodents have demonstrated that hippocampal neuronal subpopulations respond to food cues and encode food-place memory[1,2]. Projections from the lateral hypothalamus (LH) are central to this orexigenic hippocampal function, as disturbance of this circuit leads to dysregulated eating behavior[3]. These LH projections were found to express melanin-concentrating hormone (MCH)[6,7], an orexigenic neuropeptide produced in the LH area (refers to the lateral hypothalamus and its adjacencies)[3]. MCH-containing projection neurons have been reported to influence the reward value of food with MCH overexpression associated with the obese state[8–10].

The underlying circuit in which the LH and hippocampus interact, and its relevance to orexigenic appetition in humans are yet to be examined. Here, we characterize the structural and functional involvement of the human hippocampus in food-related appetition.

Orexigenic appetition within the dorsolateral hippocampus

Using probabilistic tractography in high-resolution, normative data from the 7T Human Connectome Project release (n = 178), we found that LH connections (streamlines) converge in the dorsolateral hippocampus (dlHPC) (Fig. 1A). We then investigated the functional involvement of dlHPC in the processing of a palatable taste. More specifically, we tested the following hypotheses: 1) dlHPC spectral dynamics discriminate between sweet-fat and neutral cues, and 2) spectral dynamics will differ between dlHPC and non-dlHPC contacts. We measured local field potential activity, using intracranial electrodes (n=54) implanted in the human hippocampus, while subjects (n=9) performed a sweet-fat incentive task paradigm (Fig. S1)[11–13]. Demographic and clinical characteristics of all subjects are described in Table S1. In this paradigm, individuals were cued for 1 second with an image representative of either a sweet-fat or taste-neutral solution to be subsequently delivered for consumption. We found that low-frequency

power (~4-6 Hz, condition-specific pre-stimulus normalized) in the dlHPC was significantly higher ($p < .05$, paired non-parametric cluster-based permutation testing, using null-distribution cluster size to correct for multiple comparisons) during anticipation of the sweet-fat solution compared to a neutral taste (Fig. 1B, 1C top panel). While higher frequencies may reflect more local activity, lower frequencies are thought to be advantageous in routing information across distant areas as their longer period accommodates the temporal demand of conduction velocity across multiple synaptic delays[14]. This profile was observed immediately following the cue (~ 110 ms) (Fig. 1B) and was localized to contacts within the dlHPC subregion (Fig. 1C-D). These findings suggest that dlHPC low-frequency power differentially supports anticipation of appetitive food items.

Evoked potentials support interconnections

Given that tractography cannot assess the potential monosynaptic nature of interactions between two brain regions[15], we performed direct, single-pulse, electrical stimulation (bipolar; biphasic positive; 0.5 Hz; 6mA; pulse width of 200 s; 49 trials; 120 seconds total) in a human subject with rare, if ever, recordings from both LH and sweet-fat-responsive dlHPC electrodes (Fig. 2A). Voltage deflections (or evoked potentials) are typically observed within 10-100 ms from stimulation onset when recording from a region directly connected to the stimulation site[16,17]. Following stimulation pulses to the sweet-fat-responsive dlHPC electrodes, we observed sharp and fast (~25ms) antidromic evoked potentials recorded in the single electrode within the LH area (Fig. 2B and Fig. S5 for raw, common average and bipolar re-referenced from single-trials signal in electrodes). Similar stimulation pulses encompassing the LH area electrode also resulted in fast, orthodromic, evoked potentials in the dlHPC (Fig. 2C and Fig. S6 for raw, common average and bipolar re-referenced from single-trials signal in electrodes). These bidirectional, fast, evoked potentials recorded in both regions following stimulation of the other are indicative of monosynaptic circuit-interactions between them.

MCH+ projections to dlHPC

Given that MCH is an orexigenic neuropeptide produced in the LH area with a well-described role in appetition[3,8,9], we next tested for MCH+ projections in the dlHPC subregion. To do so, we leveraged another rare opportunity afforded by a *post-mortem* sample of human tissue for the immunolabeling-enabled 3D imaging of solvent cleared organs (iDISCO) procedure (Fig. 3A). This technique allowed for 3D immunostaining and visualization of axonal projections carrying specific peptides within tissue cuboids, whereas conventional techniques would be limited in visualizing axons intersecting histological slices[18].

First, we manually identified the location of our sample in a corresponding coronal slice in the high-resolution MNI 09c template brain (Fig. S7). Second, we extracted a representative dorsolateral section that encompassed the dlHPC subregion in the template brain (Fig. 3A). This section was then processed through the iDISCO brain-clearing procedure, staining for MCH (Phoenix Pharmaceuticals, Inc and Alexa Fluor 647 Thermo Fisher). Third, the cleared and stained section was again manually overlaid to the

corresponding coronal slice of the high-resolution MNI 09c template brain with the additional overlay of the tractography-identified dlHPC subregion (Fig. 3B). We found that the dlHPC section contained MCH+ orexigenic projections visualized using the brain-clearing 3D histology (Fig. 3C; *Suppl. Video*).

LH-dlHPC connectivity implicated in obesity

A human binge eating cohort (n=34, females) was subdivided into overweight/obese (body mass index, BMI ≥ 25 m^2/kg, n=17) and lean (BMI < 25 m^2/kg, n=17) groups. We confirmed the dlHPC contained the LH-dlHPC node, previously defined by LH streamlines, by co-registering our normative hippocampal subregions of interest and the atlas-based LH (Fig. 4A) to images acquired from these human subjects. Akin to the normative cohort described above (Fig. 1A), we also found significantly higher normalized counts of LH streamlines in the left (t = -4.585; p < .001) and right (t = -3.609; p < .001) dlHPC voxels of this cohort as compared to the hippocampal voxels outside the dlHPC (i.e., non-dlHPC hippocampal voxels) (Fig. 4B).

We next assessed whether structural and functional connectivity of the LH-dlHPC circuit differ between overweight/obese and lean groups. We found that resting state functional connectivity (rsFC) between the dlHPC and LH area was significantly decreased in overweight/obese compared to lean subjects (t = 2.51; p = .018) (Fig. 4C). Probabilistic tractography-based structural connectivity index (CI, as defined by Tschentscher *et al.*[19]) between the dlHPC and the LH area was also significantly decreased in obese/overweight compared to lean groups in the left (t = 2.13; p = .042) but not right (t = 1.07; p = .295) hemispheres (Fig. 4D). We confirmed that these connectivity findings were specific to the dlHPC subregion by performing a similar analysis between the non-dlHPC hippocampal voxels and the LH area. No differences in LH-non-dlHPC structural CI nor rsFC were observed between overweight/obese and lean groups (Fig. S8).

As we were ultimately interested in the overall multivariate pattern of these functional and structural circuit alterations, we fit a multivariate logistic regression model including neuroimaging as well as behavioral variables (detailed in Online Methods) to predict whether a subject belongs to the overweight/obese or lean group. Using backwards elimination, we identified LH-dlHPC rsFC (β = -9.886, p = .044) and LH-left dlHPC CI (β = -14.676, p = .037) as the only independent predictors of obesity, with a variance inflation factor (VIF) of 1.32 (VIF < 2.5 suggests negligible collinearity between variables)[20]. Such findings further implicate this circuit in obesity involving dysregulated eating behavior.

Discussion

As a higher-order processing center involved in integrating external and internal stimuli, the hippocampus is uniquely positioned as an important node for orexigenic appetition[1,2,21]. Here, we characterized an hedonic orexigenic subnetwork within the human hippocampus. Structurally, LH streamlines converge in the dorsolateral aspect of the hippocampus (i.e., dlHPC); interconnections between the LH and dlHPC are further validated via single-pulse stimulation of the dlHPC resulting in sharp and fast voltage deflections

in the LH area. This hippocampal subregion contains MCH+ projections presumably derived from LH soma[3]. Functionally, the dlHPC exhibits specific field potential responses during anticipation of a high-caloric, sweet-fat solution. Lastly, the LH-dlHPC circuit is perturbed in patients with obesity involving dysregulated eating patterns.

The interrogation of a neural circuit underlying appetitive processing in living humans poses unique challenges, and has mostly relied on functional MRI and non-invasive electrophysiology[22–24]. For over two decades, however, *in-vivo* structural investigations of human brain circuits have been made possible by diffusion MRI-based tractography[25,26]. The key limitation of tractography is that it may be prone to false positives and negatives, and it may also not allow distinction between afferent and efferent projections[27,28]. Nonetheless, tractography findings can be supported by direct interrogation of circuits with (1) stimulation-induced evoked potentials[29] and (2) post-mortem brain clearing 3D histology[15]. Here, we used high-resolution diffusion MRI to define the hippocampal subregion where LH streamlines are more densely populated (i.e., the dlHPC). Thereafter, we also applied the two aforementioned modalities uniquely in parallel to further probe and characterize LH connections within the dlHPC.

Stimulation of either dlHPC or the LH caused fast, sharp and reproducible voltage deflections in the other region, potentially indicating monosynaptic connections between them[16]. The shapes of the evoked potentials differed depending on which node received stimulation or recordings, which may reflect cytoarchitecture differences between the two regions and the position of the electrode with regards to the tissue[17]. In a *post-mortem* hippocampal specimen, we then used iDISCO 3D histology, immunostaining for MCH, a neuropeptide that is involved in feeding and primarily synthesized in the LH and its immediate adjacencies[3,8–10], to further confirm and characterize orexigenic LH projections within the dlHPC subregion. These histologically-defined LH projections within the dlHPC subregion shed light on the directionality of the previously described evoked potentials, with the responses recorded in the LH area (following dlHPC stimulation) likely representing antidromic effects of stimulating these projections, as previously described in different subnetworks[30,31]. This dlHPC subregion was selected for functional examination with intracranial electrophysiological recordings during the sweet-fat incentive paradigm.

Comparable to our work, the same sweet-fat paradigm used here has been applied to functional MRI studies that showed increased hippocampal activation in response to sweet-fat compared to neutral stimuli[32]. In addition, hippocampal activation in response to food stimuli has been reported to be decreased following intranasal insulin administration[33]. While these studies place the human hippocampus at the intersection of energy homeostasis and appetitive processing, functional fMRI and non-invasive electrophysiology, respectively, lack the temporal and spatial resolution for uncovering differential hippocampal subregion involvement. Moreover, reports on hippocampal connectivity underlying dysregulated eating and obesity are scarce, and conspicuously absent are studies examining hypothalamic inputs in humans. Subjects undergoing brain mapping with intracranial electrophysiology provide a unique opportunity to overcome these limitations in the interrogation of specific regions of interest during controlled assays such as a food-incentive paradigm[12,13].

Intracranial electrophysiology of this dlHPC subregion revealed ~4-6 Hz discriminatory power. This frequency range overlaps with theta ranges, prominent rhythms in the both the rodent and human hippocampus ascribed to mnemonic processes including organizing events in a sequence, spatial navigation and exploration and facilitating transient interactions for memory encoding and retrieval[34,35]. Lower frequencies including theta have also been observed in neocortical areas and linked to both mnemonic and cognitive control processes[36]. The ubiquitous presence of this rhythm across areas and behavioral contexts led to a hypothesis of its more general role[37], such as mediating information transfer between the recruited regions and at temporal scales associated with a given behavioral context. Given that the hippocampus is a higher order node integrating multimodal information coming from neocortical and subcortical structures, this low frequency profile may mediate information transfer between the dlHPC and LH as well as other recruited structures recruited during food anticipation. Our report of low frequency power increase in this time window is consistent with power increase in the same frequency range in mice exposed to olfactory sweet-fat cues, reflecting a degree of generality of this signal to appetitive food anticipation irrespective of the sensory modality of the cue[1–3,38].

Previous studies have also implicated the human hippocampus and hypothalamus in dysregulated eating and obesity. Neuroimaging work reported hippocampal activation in response to food stimuli increased in children with obesity and dysregulated eating (e.g., eating in dissonance with homeostatic requirements)[39]. Other work reported a decrease in hippocampal activation in response to food images that predicts post-task levels of chocolate consumption, and abnormal hippocampal activation during reward processing in subjects with dysregulated eating behaviors[40,41]. In addition to these neuroimaging studies, hippocampal concentration of metabolites (e.g., creatine + phosphocreatine) have also been reported to be increased in obese/overweight subjects, potentially indicating BMI-related alterations in inflammatory cytokines and adipokines within the hippocampus[42]. With regards to the hypothalamus, prior work established an association between MCH overexpression and obesity in animal models[8] and neuroimaging work reported increased hypothalamic activation during a task requiring inhibitory control in subjects with dysregulated eating[43]. Only one study has reported abnormal rsFC between the LH and multiple brain regions in adolescents with excessive weight[44]; while the hippocampus was identified as functionally connected to the LH, this subnetwork's involvement in obesity was not reported. Our discovery of this link, however, is likely due to the identification of the dlHPC as the subregion of interest, as findings of decreased LH-hippocampal connectivity in the obese state were not observed when including the hippocampal voxels outside the dlHPC.

The present investigation provides evidence supporting decreased rsFC and structural connectivity between LH and dlHPC in obese/overweight females. These findings only emerged after the definition of the dlHPC as the subregion of interest, as our two cohorts showed no differences in connectivity between the non-dlHPC voxels and the LH. Moreover, the finding that functional and structural connectivity measures were significant predictors of overweight/obese *vs*. lean group assignments supports the notion that the LH-dlHPC appetitive processing node is indeed altered in the obese state. Putting these findings in context of the reports discussed above, structural and functional abnormalities involving the

MCH+ LH-dlHPC node uncovered here may predispose individuals struggling with dysregulated eating behavior to obesity.

A few considerations are noteworthy regarding the interpretations of the present findings. Firstly, we did not include males or subjects struggling with other forms of dysregulated eating. We chose to use a homogeneous female only binge eating cohort to ensure that our findings would not be skewed by sex or behavioral differences. Our electrophysiological analysis, however, are not sex specific. Secondly, directionality cannot be inferred from our cortico-subcortical evoked potential experiment, as the observed LH signal can be explained by either retrograde activity along the LH axons, or anterograde activity along the dlHPC axons. Thirdly, MCH+ projections may be coming from either the LH or its immediately adjacent structures, such as the zona incerta[45,46]. Fourthly, we had only a single case with simultaneous LH and dlHPC intracranial electrodes for the experiment with cortico-subcortical evoked potentials and a single sample for the 3D histology; together, however, these novel, complimentary methods afforded us a unique opportunity to leverage and cross-validate these approaches to interrogate a specific human orexigenic subnetwork. Lastly, what remains unclear is the extent to which the properties of the appetitive circuit identified here generalize to other hedonic behaviors.

Collectively, the convergence of modalities has elucidated a circuit that is perturbed in a disease-relevant state, furthering our understanding of how specific node interactions within the human brain are involved in obesity and related eating disorders.

abbreviations

LH = lateral hypothalamic area; MRI = magnetic resonance imaging; dlHPC = dorsolateral hippocampus; stereo-EEG = stereo-electroencephalography; fMRI = functional magnetic resonance imaging

Declarations

Acknowledgments

We thank all participants who took part in the study. We thank Austin Feng, Erik B. Lee, Dr. Rajat Shivacharan and Dr. Johnathon J. Parker for their support running the sweet-fat task incentive paradigm and acquiring the single-pulse stimulation data in the Epilepsy Monitoring Unit. We are grateful to members of the Parvizi Lab, including Dr. Josef Parvizi, Clara Sava-Segal, and Claire Perry for their invaluable support that enabled the electrophysiology data acquisition in the Epilepsy Monitoring Unit. We thank Dr. Dora Hermes for her support with the code for the analysis of the single-pulse stimulation data. We thank the Department of Neuropathology of the Stanford University School of Medicine for the post-mortem sample of the human hippocampus. In addition, we thank Dr. Anna Mathia Klawonn for her input in the staining used to identify hypothalamic orexigenic projections. We thank Hannah Welch and Zaenab Ayotola Onipede for organizing the demographic, clinical and behavioral data from the binge eating cohort used in this study. We also thank Dr. Josh Gold, Dr. John A. Wolf, and Dr. Disep Ojukwu for

their feedback on earlier versions of this manuscript and on the statistical analyses performed for this manuscript. This work was supported by Stanford Neurosurgery start-up funds including support from the John A. Blume Foundation and the William Randolph Hearst Foundation awarded to CHH. Brain and Behavior Research Foundation also provided funds awarded to CHH. Data collection and analysis was funded by grants from the National Institute of Health awarded to CB (K23 MH106794) and JAM (R01 NS095985).

Author contributions

C.H.H., C.B., B.K., Y.H., J.S.S., F.M.K., S.G., and D.A.N.B., made substantial contributions to the conceptualization and methodology of the work. D.A.N.B., S.G., J.S.S., F.M.K., A.W., Y.H., B.K., B.H., and K.J.M., contributed to data curation and formal analysis. All authors contributed to writing the original draft and provided substantially to manuscript review and editing. All authors have approved and agreed to be personally accountable for the submitted version.

Competing interests

The authors declare the following competing interests: C.H.H. receives consulting and speaking honoraria from Boston Scientific. C.H.H, D.A.N.B, S.G., Y.H. have patents related to sensing and brain stimulation for the treatment of neuropsychiatric disorders.

References

1. Azevedo, E. P. *et al.* A Role of Drd2 Hippocampal Neurons in Context-Dependent Food Intake. *Neuron* **102**, 873-886.e5 (2019).

2. Herzog, L. E. *et al.* Interaction of Taste and Place Coding in the Hippocampus. *J. Neurosci.* **39**, 3057–3069 (2019).

3. Noble, E. E. *et al.* Hypothalamus-hippocampus circuitry regulates impulsivity via melanin-concentrating hormone. *Nat. Commun.* **10**, 4923 (2019).

4. Sternson, S. M. & Eiselt, A.-K. Three Pillars for the Neural Control of Appetite. *Annu. Rev. Physiol.* **79**, 401–423 (2017).

5. Dalley, J. W. & Robbins, T. W. Fractionating impulsivity: neuropsychiatric implications. *Nat. Rev. Neurosci.* **18**, 158–171 (2017).

6. Allen Institute for Brain Science. Microarray Data. *Allen Brain Atlas* https://human.brain-map.org/microarray/search/show?exact_match=false&search_term=melanin%20concentrating%20hormone&search_type=gene (2012).

7. Sunkin, S. M. *et al.* Allen Brain Atlas: an integrated spatio-temporal portal for exploring the central nervous system. *Nucleic Acids Res.* **41**, D996–D1008 (2013).

8. Ludwig, D. S. *et al.* Melanin-concentrating hormone overexpression in transgenic mice leads to obesity and insulin resistance. *J. Clin. Invest.* **107**, 379–386 (2001).

9. Alon, T. & Friedman, J. M. Late-Onset Leanness in Mice with Targeted Ablation of Melanin Concentrating Hormone Neurons. *J. Neurosci.* **26**, 389–397 (2006).

10. Whiddon, B. B. & Palmiter, R. D. Ablation of Neurons Expressing Melanin-Concentrating Hormone (MCH) in Adult Mice Improves Glucose Tolerance Independent of MCH Signaling. *J. Neurosci.* **33**, 2009–2016 (2013).

11. Stice, E., Spoor, S., Bohon, C. & Small, D. M. Relation between obesity and blunted striatal response to food is moderated by TaqIA A1 allele. *Science* **322**, 449–452 (2008).

12. Huang, Y. *et al.* The insulo-opercular cortex encodes food-specific content under controlled and naturalistic conditions. *Nat. Commun.* **12**, 3609 (2021).

13. Kakusa, B. *et al.* Anticipatory human subthalamic area beta-band power responses to dissociable tastes correlate with weight gain. *Neurobiol. Dis.* **154**, 105348 (2021).

14. Fries, P. A mechanism for cognitive dynamics: neuronal communication through neuronal coherence. *Trends Cogn. Sci.* **9**, 474–480 (2005).

15. Leuze, C. *et al.* Comparison of diffusion MRI and CLARITY fiber orientation estimates in both gray and white matter regions of human and primate brain. *NeuroImage* **228**, 117692 (2021).

16. Matsumoto, R. *et al.* Functional connectivity in the human language system: a cortico-cortical evoked potential study. *Brain* **127**, 2316–2330 (2004).

17. Miller, K. J., Müller, K.-R. & Hermes, D. Basis profile curve identification to understand electrical stimulation effects in human brain networks. *PLoS Comput. Biol.* **17**, e1008710 (2021).

18. Renier, N. *et al.* iDISCO: a simple, rapid method to immunolabel large tissue samples for volume imaging. *Cell* **159**, 896–910 (2014).

19. Tschentscher, N., Ruisinger, A., Blank, H., Díaz, B. & Kriegstein, K. von. Reduced Structural Connectivity Between Left Auditory Thalamus and the Motion-Sensitive Planum Temporale in Developmental Dyslexia. *J. Neurosci.* **39**, 1720–1732 (2019).

20. Johnston, R., Jones, K. & Manley, D. Confounding and collinearity in regression analysis: a cautionary tale and an alternative procedure, illustrated by studies of British voting behaviour. *Qual. Quant.* **52**, 1957–1976 (2018).

21. Kanoski, S. E. & Grill, H. J. Hippocampus Contributions to Food Intake Control: Mnemonic, Neuroanatomical, and Endocrine Mechanisms. *Biol. Psychiatry* **81**, 748–756 (2017).

22. Franken, I. H. A., Huijding, J., Nijs, I. M. T. & van Strien, J. W. Electrophysiology of appetitive taste and appetitive taste conditioning in humans. *Biol. Psychol.* **86**, 273–278 (2011).

23. Chao, A. M. *et al.* Binge-eating disorder and the outcome of bariatric surgery in a prospective, observational study: Two-year results. *Obesity* **24**, 2327–2333 (2016).

24. Chao, A. M. *et al.* Sex/gender differences in neural correlates of food stimuli: a systematic review of functional neuroimaging studies. *Obes. Rev.* **18**, 687–699 (2017).

25. Conturo, T. E. *et al.* Tracking neuronal fiber pathways in the living human brain. *Proc. Natl. Acad. Sci.* **96**, 10422–10427 (1999).

26. Mori, S., Crain, B. J., Chacko, V. P. & Zijl, P. C. M. V. Three-dimensional tracking of axonal projections in the brain by magnetic resonance imaging. *Ann. Neurol.* **45**, 265–269 (1999).

27. Maier-Hein, K. H. *et al.* The challenge of mapping the human connectome based on diffusion tractography. *Nat. Commun.* **8**, 1349 (2017).

28. Grisot, G., Haber, S. N. & Yendiki, A. Diffusion MRI and anatomic tracing in the same brain reveal common failure modes of tractography. *NeuroImage* **239**, 118300 (2021).

29. Keller, C. J. *et al.* Mapping human brain networks with cortico-cortical evoked potentials. *Philos. Trans. R. Soc. B Biol. Sci.* **369**, 20130528 (2014).

30. Miocinovic, S. *et al.* Cortical Potentials Evoked by Subthalamic Stimulation Demonstrate a Short Latency Hyperdirect Pathway in Humans. *J. Neurosci.* **38**, 9129–9141 (2018).

31. Gunalan, K. & McIntyre, C. C. Biophysical reconstruction of the signal conduction underlying short-latency cortical evoked potentials generated by subthalamic deep brain stimulation. *Clin. Neurophysiol.* **131**, 542–547 (2020).

32. Stice, E., Burger, K. & Yokum, S. Caloric deprivation increases responsivity of attention and reward brain regions to intake, anticipated intake, and images of palatable foods. *NeuroImage* **67**, 322–330 (2013).

33. Guthoff, M. *et al.* Insulin Modulates Food-Related Activity in the Central Nervous System. *J. Clin. Endocrinol. Metab.* **95**, 748–755 (2010).

34. Buzsáki, G. Theta rhythm of navigation: link between path integration and landmark navigation, episodic and semantic memory. *Hippocampus* **15**, 827–840 (2005).

35. Nyhus, E. & Curran, T. Functional role of gamma and theta oscillations in episodic memory. *Neurosci. Biobehav. Rev.* **34**, 1023–1035 (2010).

36. Cavanagh, J. F. & Frank, M. J. Frontal theta as a mechanism for cognitive control. *Trends Cogn. Sci.* **18**, 414–421 (2014).

37. Mitchell, D. J., McNaughton, N., Flanagan, D. & Kirk, I. J. Frontal-midline theta from the perspective of hippocampal 'theta'. *Prog. Neurobiol.* **86**, 156–185 (2008).

38. Samerphob, N., Cheaha, D., Chatpun, S. & Kumarnsit, E. Hippocampal CA1 local field potential oscillations induced by olfactory cue of liked food. *Neurobiol. Learn. Mem.* **142**, 173–181 (2017).

39. Mestre, Z. L. *et al.* Hippocampal atrophy and altered brain responses to pleasant tastes among obese compared with healthy weight children. *Int. J. Obes.* **41**, 1496–1502 (2017).

40. Lyu, Z. & Jackson, T. Acute Stressors Reduce Neural Inhibition to Food Cues and Increase Eating Among Binge Eating Disorder Symptomatic Women. *Front. Behav. Neurosci.* **10**, 188 (2016).

41. Cyr, M. *et al.* Reward-Based Spatial Learning in Teens With Bulimia Nervosa. *J. Am. Acad. Child Adolesc. Psychiatry* **55**, 962-971.e3 (2016).

42. Bond, D. J. *et al.* Diagnosis and body mass index effects on hippocampal volumes and neurochemistry in bipolar disorder. *Transl. Psychiatry* **7**, e1071–e1071 (2017).

43. Lock, J., Garrett, A., Beenhakker, J. & Reiss, A. L. Aberrant Brain Activation During a Response Inhibition Task in Adolescent Eating Disorder Subtypes. *Am. J. Psychiatry* **168**, 55–64 (2011).

44. Martín-Pérez, C., Contreras-Rodríguez, O., Vilar-López, R. & Verdejo-García, A. Hypothalamic Networks in Adolescents With Excess Weight: Stress-Related Connectivity and Associations With Emotional Eating. *J. Am. Acad. Child Adolesc. Psychiatry* **58**, 211-220.e5 (2019).

45. Bittencourt, J. C. *et al.* The melanin-concentrating hormone system of the rat brain: an immuno- and hybridization histochemical characterization. *J. Comp. Neurol.* **319**, 218–245 (1992).

46. Hahn, J. D. Comparison of melanin-concentrating hormone and hypocretin/orexin peptide expression patterns in a current parceling scheme of the lateral hypothalamic zone. *Neurosci. Lett.* **468**, 12–17 (2010).

online methods

MRI data and preprocessing. MRI acquisition parameters are summarized in Table S2. We included MRI data from three different cohorts: (1) normative diffusion MRI dataset from 178 unrelated subjects from the HCP who underwent a ultra-high-resolution acquisition on a "Magnetom" 7T MRI scanner (Siemens Medical Systems, Erlangen, Germany) were obtained from the publicly available S1200 WashU-Minn-Ox HCP dataset[1–3]; (2) functional resting-state, and diffusion MRI data from 34 binge-prone females

recruited by the Stanford Eating Disorders Program on a 3T MRI scanner (Discovery MR750, GE Healthcare, Milwaukee, Wisconsin).

Resting-state fMRI scans from the binge-prone cohort were preprocessed using fMRIPrep 1.2.3[4]. In brief, the preprocessing of the functional image involved skull-stripping, co-registration to the T1 reference image, and head motion and susceptibility distortion corrections. After removal of non-steady state volumes and spatial smoothing with a 6mm FWHM isotropic Gaussian kernel, ICA-AROMA was used to identify motion-related noise components in the BOLD signal[5]. Framewise displacement (FD) and root mean square variance over voxels of the temporal derivative of time courses (DVARS) were calculated[6,7]. Global signals were extracted within the cerebrospinal fluid (CSF), white matter (WM), gray matter (GM), and whole-brain masks. XCP Engine 1.0 was used to perform denoising of the preprocessed BOLD output from fMRIPrep, utilizing the estimated confound parameters[8,9]. This included demeaning and removal of any linear or quadratic trends and temporal filtering using a first-order Butterworth bandpass filter (0.01-0.08 Hz). These preliminary preprocessing steps were then followed by confound regression of ICA-AROMA noise components, together with mean WM, CSF, and global signal regressors. All regressors were bandpass filtered to retain the same frequency range as the data to avoid frequency-dependent mismatch[8]. Whereas preprocessing was performed on the diffusion MRI data from the binge-prone cohort to prepare the images for probabilistic tractography using the FSL suite[10,11], the normative HCP diffusion MRI data had already been preprocessed (with the minimal preprocessing pipeline). The diffusion-weighted images were corrected for motion and geometric distortions using the 'topup' and 'eddy' functions, similar to that applied in HCP's preprocessing pipeline. For each subject, diffusion and T1-weighted images were co-registered using boundary-based registration.

Probabilistic tractography. Probabilistic tractography was used to evaluate the connections between LH and hippocampus. The LH mask was defined on the standard T1 MNI152 09c template adapted from CIT168 Subcortical In Vivo Probabilistic Atlas[12], while the hippocampi masks were defined using the Harvard-Oxford brain atlas. This registration was performed using Advanced Normalization Tools (ANTs), which consists of two successive steps of linear and nonlinear registration between the subject's brain and the MNI brain. In a third step, the MNI-defined ROIs were registered to the subject's space. FSL's Bayesian Estimation of Diffusion Parameters Obtained using Sampling Techniques (BEDPOSTX) was used to conduct Monte Carlo sampling of probability distribution of diffusion parameters at each voxel, accounting for up to three crossing fibers directions within a voxel[13]. Fiber tracking was performed with FSL's Probtrackx2, using distance correction and each hippocampal voxel as seed and the LH as target[14]. A total of 5000 seed points were used to generate streamlines from each seed voxel, and only the streamlines that reached the target were retained for further analysis. The results of Probtrackx are summarized in a map of "streamline probability" and "waytotal", representing the probability for each seed voxel to reach the target and the total number of streamlines from a given seed that reached the target, respectively. The strength of the connections between seed and target was calculated as a tractography connectivity index (tractography-CI), as defined in a previous study by the formula: log(waytotal)/log(5000 x Vseed)[15]. The waytotal resulting from the tractography was log-transformed

and divided by the log-transformed product of the generated sample streamlines in each seed voxel (5000) and the number of voxels in the respective seed mask (Vseed). The log-transformation increased the likelihood of reaching normality, which was tested using the Shapiro-Wilk test[16].

Hippocampal segmentation. Tractography was used to generate a probabilistic map each with voxel's streamline probability to the LH for all 178 subjects from the normative HCP dataset. Each subjects' streamline probability map to the LH was transformed to standard MNI 09c space so that they could be averaged and concatenated into a normative weighted average group map of streamline probability between the hippocampal area and the LH across the 178 HCP subjects. We performed this analysis to define the hippocampal subregions in the normative HCP data and then applied these subregions to the binge-prone cohort. We then used k-means to segment group average hippocampus streamline probability maps. This hypothesis-free method uses successive iterations to assign each voxel to one of two clusters, without the application of external spatial constraints. For the case of large inter-voxel similarities in streamline count, the algorithm fails to identify two distinct clusters. Resulting clusters represented normative hippocampal subregions based on its connectivity to the LH in standard MNI 09c space. Finally, we co-registered the normative clusters to the MRI images from our subjects implanted with depth electrodes as well as the binge eating cohort.

Sweet-fat incentive paradigm. Participants (n=9, Table S1) underwent surgical implantation of depth electrodes for neurosurgical epilepsy monitoring. The location of electrode implantation was determined solely based on clinical needs and thus varied across participants. The inclusion criteria for this study were the presence of at least one hippocampal depth electrode. Consent to participate in this study was obtained according to the Declaration of Helsinki and approved by the institutional ethical committee. We have adapted the sweet-fat incentive paradigm, also known as the Milkshake task[17] for intracranial electrographic recordings during cued anticipation and consumption of a sweet-fat and a taste-neutral solution, as previously published and described in detail by our group[18,19]. Data acquisition and experimental task were previously described[18]. Briefly, neural activity was sampled at 1024 Hz from AdTech electrodes while subjects engaged in a sweet-fat incentive computer-based paradigm (Fig. S1). Each trial in this paradigm began with a 2-sec fixation cross presented on a computer screen - this period is referred to as the pre-stimulus period. This was followed by a 1-sec presentation of an image of a glass of either water or of milkshake, which served as a cue for the solution to be subsequently delivered through a mouthpiece to the subject for consumption. Before the solution was delivered, a 2-sec image of a fixation cross was viewed. The 1-sec presentation of the solution to be delivered and this 2-sec fixation cross period are referred to as an anticipatory period (3-sec). Following the anticipatory period is a 5-sec receipt/consummatory period, consisting of a 3-sec solution delivery period followed by a 2-sec consumption of solution period. Sweet-fat and taste-neutral trials were presented in a randomized order, with a total of 80 to 100 trials evenly split between sweet-fat and taste-neutral conditions. Upon task completion, the participants were asked to rate on a 1-10 Likert scale the quality of the sweet-fat solution (Likert scale, 1–10) and which solution (sweet-fat vs. taste-neutral) they preferred.

Electrode localization. Pre-surgical MRI scan was co-registered to post-surgical CT scan for electrode visualization and localization as described previously[20]. Locations of depth electrodes within the medial temporal lobe were then examined by one rater with expertise in medial temporal lobe anatomy in neuroimaging (D.A.N.B). Electrodes in direct contact with the hippocampal area were selected for further evaluation. Then, we co-registered the normative hippocampal clusters (i.e., dlHPC and non-dlHPC) that we had previously defined in standard MNI09c template brain to each subject's native space (Fig. 1D). All hippocampal electrodes (n=54) were labelled according to whether they were in direct contact with dlHPC or not (i.e., non-dlHPC). This localization was performed prior to time-frequency analysis.

Task data preprocessing and analyses. Electrophysiological data was downsampled to 1000 Hz, notch filtered for 60 Hz and 2nd-3rd harmonics, and Laplacian re-referenced in FieldTrip as previously described[18,19]. Artifact timepoints were defined as voltage values greater or less than the mean signal of all 10-sec trials concatenated, recorded from the same channel plus 4 multiples of its standard deviation. Any trial with at least 1 detected artifact timepoint was excluded. Time-Frequency analysis was implemented using the wavelet toolbox in Matlab. There are three input parameters: 1) minimum frequency, set to 3, 2) maximum frequency, set to 250, and 3) NumVoices, set to 32. The toolbox generates 'scales' based on the desired frequency range (defined by min to max frequencies), which then get mapped into frequencies. The trial vector, scales vector, and 'morl' are inputs to the cwtft function in matlab, which generates the wavelets and power extraction. Wavelets were first tested on ground truth data with known spectral properties before use on experimental data.

Trial instantaneous power values were normalized to power at the same frequency and channel during the 1-sec prestimulus period across all trials in the same condition (condition specific pre-stimulus normalization). The prestim duration of any trial with at least 1 detected artifact timepoint was excluded from the normalizing distribution (see previous section). Condition specific pre-stimulus normalization was used to account for possible differences in baseline power before stimulus presentation. Results were reproduced using an alternative normalization method whereby power values were normalized relative to the distribution of power in the same frequency and channel, during the entire recording.

Spectral analyses were primarily focused on the anticipation period (1-sec cue, and 2-sec post-cue fixation). Statistical differences in time-frequency power between conditions were calculated using cluster-based permutation testing[21]. Briefly, this involved calculating a t-statistic in each time-frequency voxel, between the two conditions (sweet fat vs. neutral), thereby generating the observed t-map. The distribution for each voxel was generated by pooling the time-frequency maps from all channels and subjects (trials were averaged to generate a single map per channel). The observed t-map was then compared to a null distribution (shuffled condition labels) of t-maps generated over 1000 paired permutations. A p-value for each voxel was obtained by comparing the observed to the null t-value at the same time-frequency voxel, thereby generating a p-map. Clusters of contiguous voxels with a $p < .05$ were identified and compared to the null-distribution cluster size. Observed clusters with sizes larger than the 95th percentile of those from the null distribution were considered significant after correction for multiple comparisons.

Evoked potentials. As previously described, we performed single-pulse stimulations at rest using an intracranial electrical waveform generator and switchbox[22,23] (MS-120BK-EEG and PE-210AK, Nihon Kohden, Tokyo, Japan). Electrical stimulation was delivered through adjacent pairs of electrodes in biphasic pulses (6mA; 200 μs/phase, 49 trials) at a frequency of 0.5 Hz for a total of 120 seconds. We measured electrical potentials in response to stimulation with a video EEG monitoring system using a sampling rate of 2000 Hz (version WEE-1200, Nihon Kohden). We analyzed the single-pulse stimulation data using custom Matlab scripts. We first applied a high-pass butterworth filter (1 Hz) to exclude slow varying effects and segmented evoked responses time series from recording channels were into 2500 ms epochs time-locked to stimulus onset (500 ms pre-stimulus and 2000 ms post-stimulus). Then, we re-referenced the data to the common average signal, excluding stimulated channels, channels with artifacts, and channels with large, evoked responses, as previously described[24]. Finally, to exclude potential effects of pre-stimulus signal fluctuations, we applied a baseline correction by subtracting the average signal between 200 ms and 20 ms prior to stimulus onset. To ensure that these preprocessing steps did not introduce a bias, we also provided line traces of bipolar re-referenced and the single-trials raw signal from the recording electrodes (Fig. S5).

Human hippocampal sample. In accordance with the local IRB, a post-mortem sample of the left hippocampal area (Fig. 2C, left panel) was obtained from a whole brain with no known pathologies that had been extracted 24 hours after death and placed in 10% formalin for one day. The sample was perfused and stored in PFA 4%. For the brain-clearing procedure, we extracted a representative dorsolateral hippocampal section (Fig. 2C, mid panel) and transferred the sample to 1M phosphate-buffered saline (PBS). The sample was stored at 4°C until the iDISCO protocol was performed.

Antibody validation protocol. A validation protocol was performed to be sure that the anti-MCH (Phoenix Pharmaceuticals, Inc- USA, H070-47, Lot No. 01629-10) was compatible with the reagents used in the immunolabeling-enabled 3D imaging of solvent cleared organs (iDISCO) protocol[25]. Slices were obtained on a Vibratome at 60 μM in 1M phosphate-buffered saline (PBS) solution. The free-floating sections were permeabilized for 3 hours with methanol at room temperature and after were rinsed two times with PBS for 20 min and then rinsed with PBS with 2% TritonX-100. The sections were then incubated with permeabilization solution, PBS with 0.2% Triton, during 30 min and blocking solution, PBS with 0.2% TritonX-100, 10% DMSO, and 6% Donkey Serum for 1 hour. The anti-MCH was incubated 1:500 in PTwH (PBS with 0.2% Tween-20, 1% Heparin (10mg/ml), 0.2% Sodium Azide), overnight at -4°C. The samples were rinsed 3 times for 5 minutes and the secondary antibody, Alexa Fluor 647 anti-Rabbit (ThermoFischer Scientific-USA, A-31573) were incubated 1:250 in PTwH and 3% Donkey serum and 0.2% Sodium azide during 1 hour at RT, covered by the light. Finally, the samples were rinsed in PTwH 3 times for 5 minutes and the slices were mounted with DAPI (Vectashiels-VECTOR, USA). Images were acquired with confocal microscopy (data not shown).

iDISCO brain-clearing 3D histology. After antibody validation, we selected a representative dorsolateral section for the iDISCO protocol to confirm our hippocampal area segmentation (Fig. 1A). The section was approximately 1.0 x 0.8 x 0.4 cm and was pretreated with methanol following the iDISCO protocol[25] using

a modified immunostaining protocol. The sample was rinsed with PBS with 2% TritonX-100 two times for 1 hour. We incubated the sample in permeabilization solution, PBS with 0.2% Triton, for 30 min, and blocking solution, PBS with 0.2% TritonX-100, 10% DMSO, and 6% Donkey Serum, for 1 hour. The sample was incubated with 1:500 anti-MCH in PTwH (PBS, 0.2% Tween-20, 1% Heparin 10mg/ml, 0.2% Sodium Azide) for 10 days, nutating at 37° C. After 10 days, the samples were rinsed 3 times for 5 minutes and then every few hours and left nutating at room temperature overnight. On the next day, the sample was incubated in the secondary antibody, Alexa Fluor 647 anti-Rabbit (ThermoFischer scientific-USA, A-31573), 1:250 in PTwH and 3% Donkey serum and 0.2% Sodium azide at 37°C, nutating for 10 days, covered from light. Following secondary incubation, the sample was again rinsed in PTwH for 2 days, and the iDISCO clearing protocol was followed (https://idisco.info/idisco-protocol/update-history/)

Histological assessment of lateral hypothalamic connections in the dorsolateral hippocampus. The iDISCO brain-clearing 3D histology results were used to confirm the hippocampal area segmentation. The anti-MCH was used to identify orexigenic projections within our hippocampal sample. We assessed whether our sample from the dorsolateral hippocampal subregion, defined based on the higher number of probabilistic tractography streamlines, contained projections expressing MCH, an orexigenic neuropeptide primarily produced in the LH area. First, we manually identified the location of our whole sample in a corresponding coronal slice in the high-resolution MNI 09c template brain (Fig. S7) and then extracted a representative dorsolateral section that overlapped with the dlHPC (Fig. 2C). Following immunolabeling and clearing, the final MCH-stained sample was again manually overlaid to the corresponding coronal slice in the high-resolution MNI template brain and the tractography-based hippocampal probability map of LH area streamlines (Fig. 2D).

Demographics, clinical and behavioral data of binge-prone cohorts. Subjects' consent was obtained according to the Declaration of Helsinki and approved by the institutional ethical committee (IRB-35204). We analyzed the available clinical and behavioral data from 34 binge-prone females, defined by at least one weekly episode of eating large amounts of food in short periods accompanied by the feeling of loss of control eating over the prior 6 months (i.e., binge-prone cohort; mean age = 26 ± 5.6 years; BMI = 27.9 ± 8.5; binge frequency = 2.7 ± 1.4 episodes/week)[26]. The number of binge-eating episodes per week was assessed with the Eating Disorder Examination, a standardized diagnostic interview[27]. The Beck Depression Inventory (BDI) and the Beck Anxiety Inventory (BAI) were used to screen for depression and anxiety, respectively[28,29]. The Difficulties in Emotion Regulation Scale was used to assess impairment in emotion regulation[30]. The binge-eating-cohort was divided into two subgroups: (1) lean (n=17): BMI < 25 (referred to as lean group); (2) overweight/obese (n=17): BMI > 25 (referred to as obese/overweight group).

Resting-state functional connectivity analysis. Resting-state functional connectivity analysis was performed on the binge-prone cohort's preprocessed resting-state fMRI data using DPABI 4.3/DPARSF which is based on Statistical Parametric Mapping (SPM12, https://www.fil.ion.ucl.ac.uk/spm)[31]. Three subjects were excluded due to excessive movement as measured by 1) mean FD > 0.2mm, 2) more than

20% of FD over 0.2mm, or 3) any FD > 5mm[9]. A seed-based approach was performed to examine rsFC in the binge-prone cohort (n=34) by calculating the rsFC between the LH mask as defined above and each tractography-identified hippocampal subregion. Functional connectivity values were extracted for all subjects and utilized in further correlational analyses.

Statistical analyses. Statistical analyses were performed using the RStudio Version 1.2.5042 (RStudio, Inc.). Given the sensitivity of metrics derived from resting-state fMRI and diffusion MRI proneness to numerical distortions related to data acquisition or analytical pipeline, we employed the Tukey's method to remove outliers for each connectivity metric. After checking for normality, we then used the Student's T-test to compare rsFC as well as tractography-CI between hippocampal subregions and LH in overweight/obese and lean group. One outlier was identified and removed from the obese binge eating group and two outliers were identified and removed from the lean group in both the rsFC and structural CI analyses in Figures 3C and 3D (left panel), respectively. Additionally, we identified and removed one outlier from the lean group in the CI analysis in Figure 3D (right panel). Mann–Whitney U Test was used to compare the corrected number of streamlines between the LH and hippocampal subregions in the binge-prone cohort. To assess potential effect of confounders in the identified connectivity differences between the obese and lean group, we fit a multivariate logistic regression model to predict whether a subject belongs to the overweight/obese or lean group including the available demographic and behavioral variables in addition to the LH-dlHPC connectivity measurements. The comprehensive list of variables included: age, depression (BDI), anxiety (BAI), binge frequency, restrained eating, emotional eating and externally driven eating scores (from DEBQ), LH-dlHPC-LH rsFC, LH-non-dlHPC rsFC, LH-dlHPC structural connectivity, and LH-non-dlHPC structural connectivity. We then used backwards elimination to identify which combination of variables provided highest predictive power with the lowest total number of explanatory variables to avoid over-fitting (Akaike Information Criterion). Finally, a variance inflation factor was calculated to assess potential correlations between explanatory variables[32]. Significance was defined by $p < 0.05$ for all tests.

Data availability. Anonymized data that support the findings of this study as well as the code and materials used for analyses are available from the corresponding author upon reasonable request**.**

Online References

1. Van Essen, D. C. *et al.* The Human Connectome Project: a data acquisition perspective. *NeuroImage* **62**, 2222–2231 (2012).

2. Glasser, M. F. *et al.* The minimal preprocessing pipelines for the Human Connectome Project. *NeuroImage* **80**, 105–124 (2013).

3. Sotiropoulos, S. N. *et al.* Advances in diffusion MRI acquisition and processing in the Human Connectome Project. *NeuroImage* **80**, 125–143 (2013).

4. Esteban, O. *et al.* fMRIPrep: a robust preprocessing pipeline for functional MRI. *Nat. Methods* **16**, 111–116 (2019).

5. Pruim, R. H. R. *et al.* ICA-AROMA: A robust ICA-based strategy for removing motion artifacts from fMRI data. *NeuroImage* **112**, 267–277 (2015).

6. Power, J. D., Barnes, K. A., Snyder, A. Z., Schlaggar, B. L. & Petersen, S. E. Spurious but systematic correlations in functional connectivity MRI networks arise from subject motion. *NeuroImage* **59**, 2142–2154 (2012).

7. Power, J. D. *et al.* Methods to detect, characterize, and remove motion artifact in resting state fMRI. *NeuroImage* **84**, 320–341 (2014).

8. Ciric, R. *et al.* Benchmarking of participant-level confound regression strategies for the control of motion artifact in studies of functional connectivity. *NeuroImage* **154**, 174–187 (2017).

9. Parkes, L., Fulcher, B., Yücel, M. & Fornito, A. An evaluation of the efficacy, reliability, and sensitivity of motion correction strategies for resting-state functional MRI. *NeuroImage* **171**, 415–436 (2018).

10. Smith, S. M. *et al.* Advances in functional and structural MR image analysis and implementation as FSL. *NeuroImage* **23 Suppl 1**, S208-219 (2004).

11. Andersson, J. L. R., Skare, S. & Ashburner, J. How to correct susceptibility distortions in spin-echo echo-planar images: application to diffusion tensor imaging. *NeuroImage* **20**, 870–888 (2003).

12. Pauli, W. M., Nili, A. N. & Tyszka, J. M. A high-resolution probabilistic in vivo atlas of human subcortical brain nuclei. *Sci. Data* **5**, 180063 (2018).

13. Behrens, T. E. J., Berg, H. J., Jbabdi, S., Rushworth, M. F. S. & Woolrich, M. W. Probabilistic diffusion tractography with multiple fibre orientations: What can we gain? *NeuroImage* **34**, 144–155 (2007).

14. Jenkinson, M., Beckmann, C. F., Behrens, T. E. J., Woolrich, M. W. & Smith, S. M. FSL. *NeuroImage* **62**, 782–790 (2012).

15. Tschentscher, N., Ruisinger, A., Blank, H., Díaz, B. & Kriegstein, K. von. Reduced Structural Connectivity Between Left Auditory Thalamus and the Motion-Sensitive Planum Temporale in Developmental Dyslexia. *J. Neurosci.* **39**, 1720–1732 (2019).

16. Royston, P. Approximating the Shapiro-Wilk W-test for non-normality. *Stat. Comput.* **2**, 117–119 (1992).

17. Stice, E., Spoor, S., Bohon, C. & Small, D. M. Relation between obesity and blunted striatal response to food is moderated by TaqIA A1 allele. *Science* **322**, 449–452 (2008).

18. Huang, Y. *et al.* The insulo-opercular cortex encodes food-specific content under controlled and naturalistic conditions. *Nat. Commun.* **12**, 3609 (2021).

19. Kakusa, B. *et al.* Anticipatory human subthalamic area beta-band power responses to dissociable tastes correlate with weight gain. *Neurobiol. Dis.* **154**, 105348 (2021).

20. Liu, S. & Parvizi, J. Cognitive refractory state caused by spontaneous epileptic high-frequency oscillations in the human brain. *Sci. Transl. Med.* **11**, eaax7830 (2019).

21. Cohen, M. X. *Analyzing Neural Time Series Data: Theory and Practice*. (The MIT Press, 2019).

22. Keller, C. J. *et al.* Mapping human brain networks with cortico-cortical evoked potentials. *Philos. Trans. R. Soc. B Biol. Sci.* **369**, 20130528 (2014).

23. Shine, J. M. *et al.* Distinct Patterns of Temporal and Directional Connectivity among Intrinsic Networks in the Human Brain. *J. Neurosci.* **37**, 9667–9674 (2017).

24. Miller, K. J., Müller, K.-R. & Hermes, D. Basis profile curve identification to understand electrical stimulation effects in human brain networks. *PLoS Comput. Biol.* **17**, e1008710 (2021).

25. Renier, N. *et al.* iDISCO: a simple, rapid method to immunolabel large tissue samples for volume imaging. *Cell* **159**, 896–910 (2014).

26. American Psychiatric Association. *Diagnostic and Statistical Manual of Mental Disorders*. (American Psychiatric Association, 2013). doi:10.1176/appi.books.9780890425596.

27. Fairburn, C. G. & Cooper, Z. The Eating Disorder Examination (12th edition). in *Binge eating: Nature, assessment, and treatment* 317–360 (Guilford Press, 1993).

28. Beck, A. T., Ward, C. H., Mendelson, M., Mock, J. & Erbaugh, J. An Inventory for Measuring Depression. *Arch. Gen. Psychiatry* **4**, 561–571 (1961).

29. Beck, A. T., Epstein, N., Brown, G. & Steer, R. A. An inventory for measuring clinical anxiety: psychometric properties. *J. Consult. Clin. Psychol.* **56**, 893–897 (1988).

30. Gratz, K. L. & Roemer, L. Multidimensional Assessment of Emotion Regulation and Dysregulation: Development, Factor Structure, and Initial Validation of the Difficulties in Emotion Regulation Scale. *J. Psychopathol. Behav. Assess.* **26**, 41–54 (2004).

31. Yan, C.-G., Wang, X.-D., Zuo, X.-N. & Zang, Y.-F. DPABI: Data Processing & Analysis for (Resting-State) Brain Imaging. *Neuroinformatics* **14**, 339–351 (2016).

32. Johnston, R., Jones, K. & Manley, D. Confounding and collinearity in regression analysis: a cautionary tale and an alternative procedure, illustrated by studies of British voting behaviour. *Qual. Quant.* **52**, 1957–1976 (2018).

Supplemental Video

The Supplemental Video is not available with this version

Figures

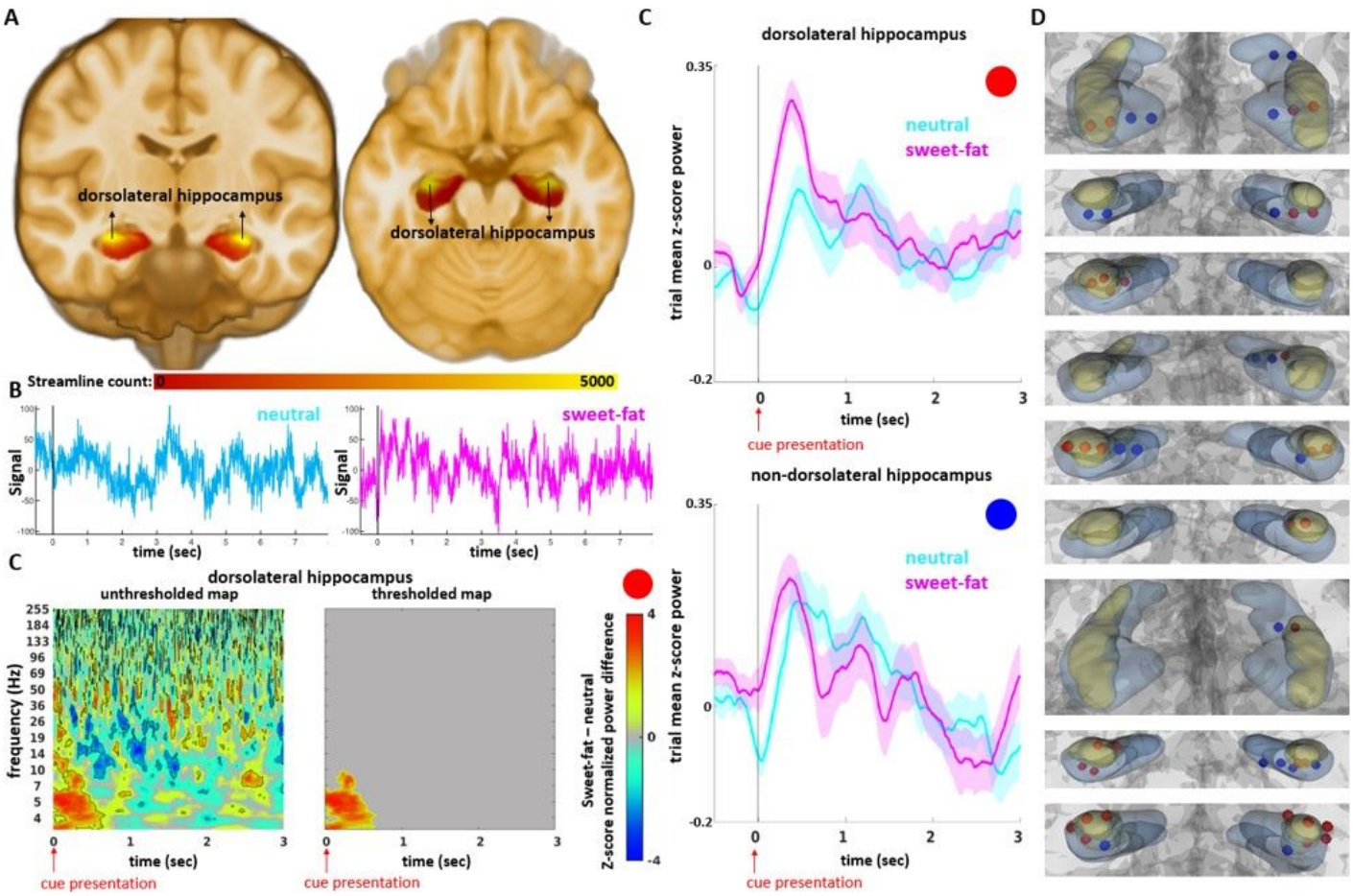

Figure 1

dlHPC subregion involvement in appetitive food processing. (A) Tractography on high-resolution, normative data from 178 HCP subjects showed that LH-hippocampal area interconnections (i.e., streamlines) converge in the dlHPC (yellow). (B) Example traces of electrophysiological time-domain recordings from the dlHPC in one subject during a taste-neutral (top, cyan) and sweet-fat (bottom, magenta) trial. The time interval displayed includes the pre-cue period (-0.5 to 0 sec), cue presentation (0-1 sec), fixation cross (1-3 sec), solution delivery (3-5 sec), fixation cross (5-6 sec), and a portion of solution receipt (6-7.5 sec). (C) z-score normalized difference spectrograms (sweet-fat minus neutral solution) in the dlHPC. Color bar indicates mean z-score power difference (using pooled channels as observations) between the two conditions compared to a null distribution. Outlined clusters (left) reflect significant contiguous time-frequency voxels ($p < .05$, cluster-based permutation testing, 1000 permutations) before correction for multiple comparisons. Thresholded map (right) displays significant

time-frequency clusters after correction for multiple comparisons. (D) 4-6 Hz mean z-score power time traces during cue (0-1 sec) and post-cue anticipation (1-3 sec) of sweet-fat (magenta) and taste-neutral (cyan) solutions, in the dlHPC (top) and non-dlHPC (bottom) hippocampal sites. 0- and 1- sec reflect cue and fixation cross image presentation times, respectively. (E) Hippocampal coverage per subject (n = 9). Red contacts indicate the contacts in direct contact with the dlHPC (yellow subregion).

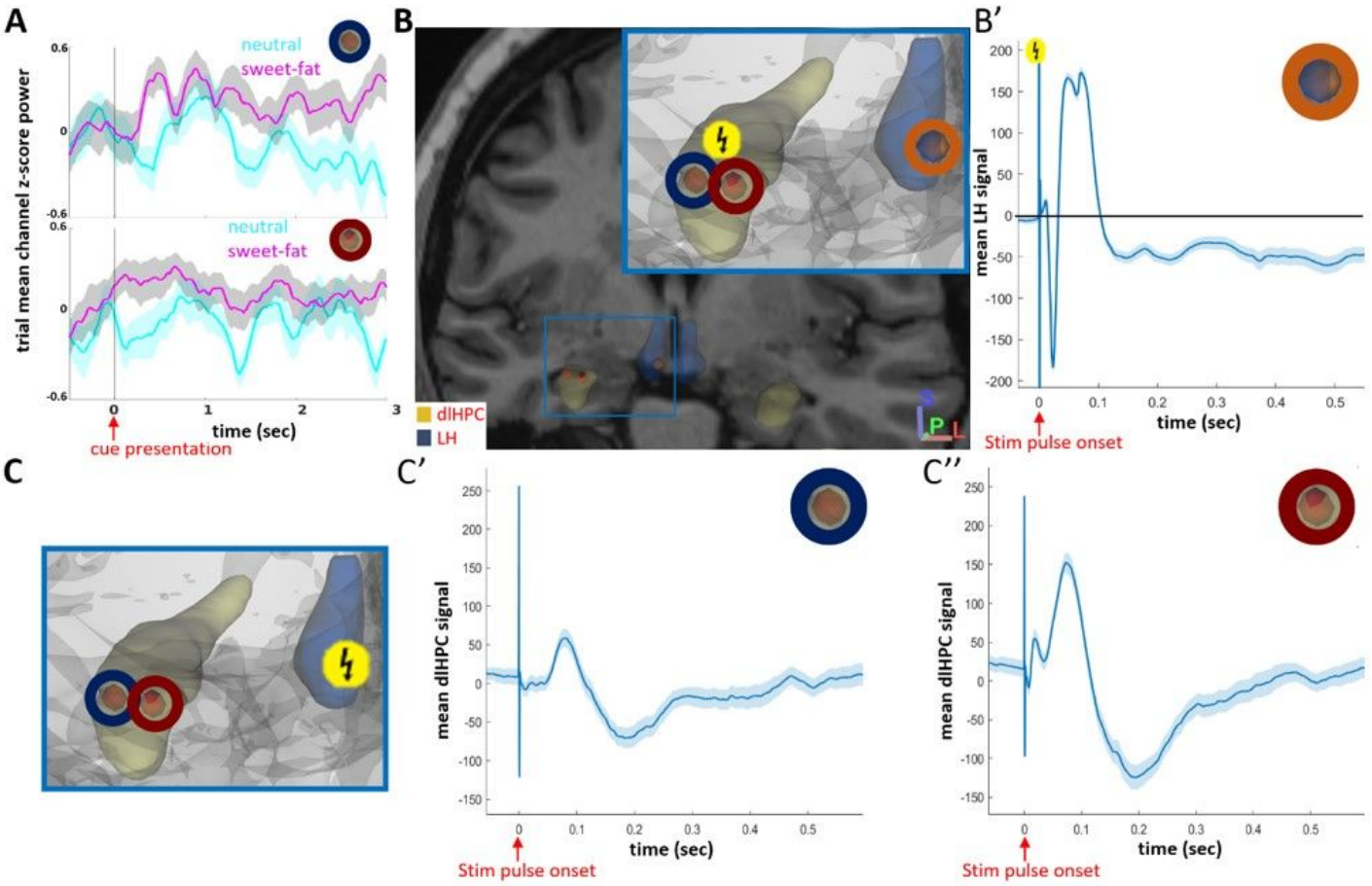

Figure 2

Dissecting the human LH–dlHPC appetitive processing circuit with single-pulse stimulation. (A) 4-6 Hz mean dlHPC (2 channels; top and bottom panels) z-score (relative to condition specific prestimulus distributions) power time traces during cue (0-1 sec) and post-cue anticipation (1-3 sec) of sweet-fat (magenta) and neutral (cyan) tastes from one subject with electrodes implanted in both dlHPC and LH area. (B) Anatomical location of simultaneous dlHPC (yellow volume) and LH area (blue volume) coverage. dlHPC sweet-fat-responsive electrodes are outlined in red and dark blue circles (same electrodes as in A) and an LH electrode is outlined in orange (same electrodes as in right panel). (B') Fast voltage deflections (~25 ms) in evoked potentials (mean +/- SEM; 49 trials) recorded from the LH electrode during bipolar stimulation of the dlHPC electrode pair. (C) The LH area (blue volume) was also stimulated with recordings in the two electrodes in the dlHPC (red and dark blue circles). (C' and C") Fast voltage deflections in evoked potentials (mean +/- SEM; 49 trials) recorded from the two same dlHPC electrodes during bipolar stimulation encompassing the LH (blue volume).

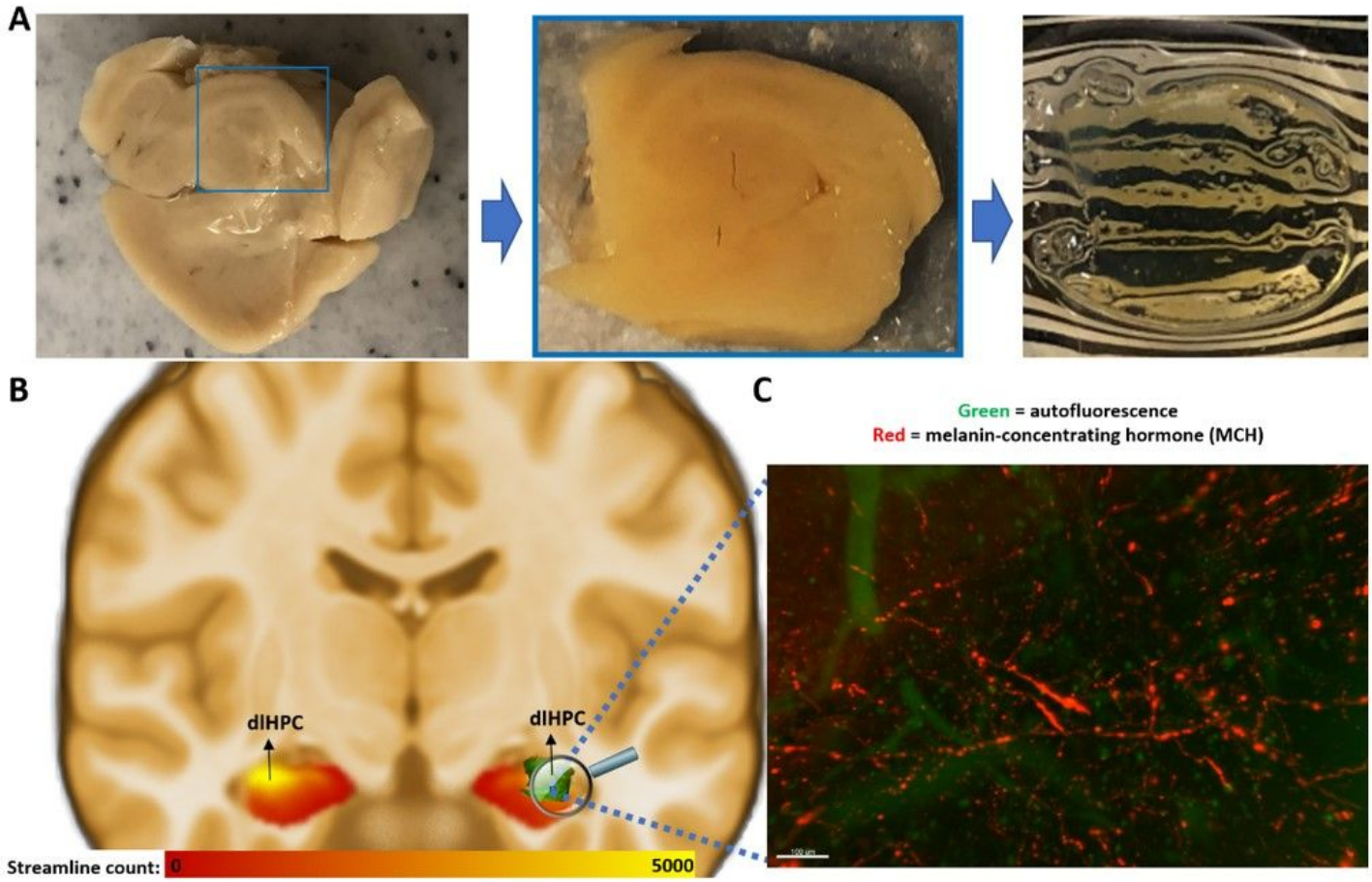

Figure 3

Dissecting the human LH–dlHPC appetitive processing circuit with 3D histology. (A) Post-mortem human sample (left panel) of the hippocampus, dlHPC section (middle panel) that was selected for iDISCO brain-clearing (right panel) procedure. (E) The iDISCO cleared section (green) was overlaid to the group average dlHPC (yellow), defined based on its higher number of LH streamlines. (F) Staining for MCH+ (Phoenix Pharmaceuticals, Inc and Alexa Fluor 647 Thermo Fisher) appears in red and autofluorescence in green within the dlHPC hotspot (high streamline probability with the LH area). Image acquired with light sheet microscope (UltraMicroscope II, Miltenyi BioTec, Germany). Scale bar=100um. See *Supplementary Video* for 3D visualization.

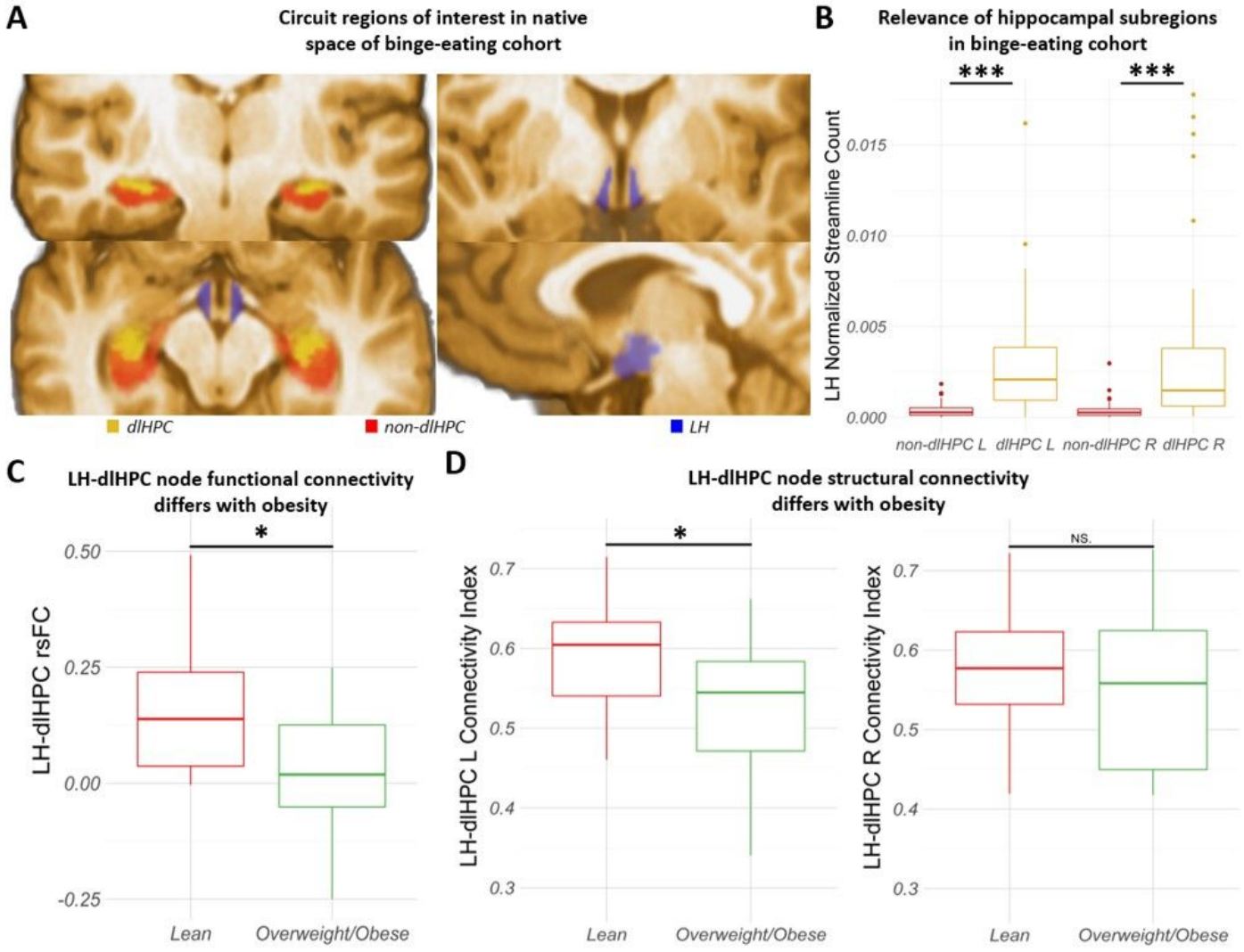

Figure 4

This circuit is associated with the obese state involving dysregulated eating behavior in humans. A) Regions of interest co-registered to native space of an exemplary subject: dlHPC (yellow, hotspot), non-dlHPC (red) and LH (blue, adapted from CIT168 Subcortical In Vivo Probabilistic Atlas). (B) Significantly higher normalized streamline counts observed between the LH and left dlHPC (t = -4.585; p < .001) and right dlHPC (t = -3.609; p < .001) compared to the non-dlHPC in the overall cohort. (C) rsFC between the dlHPC and LH was decreased in overweight/obese compared to the lean group (t = 2.51; p = .018). (D) Structural CI between the left dlHPC and LH was significantly decreased (t = 2.13; p = .042) in overweight/obese compared to lean group. No significant differences (t = 1.07; p = .295) in structural CI between the right dlHPC and LH were found (see Fig. S9 for individual subject data points for B-D). NS. = non-significant. * = p < .05. ** = p < .01. *** = p < .001.

Supplementary Files

This is a list of supplementary files associated with this preprint. Click to download.

- SupplementalMaterial.docx